

# Numerical Computation of Distortions in Magnetic Fields and Induced Currents in Physiological Solutions Produced by Microscope Objectives

Indira Chatterjee,<sup>1\*</sup> Noha Hassan,<sup>2</sup> Gale L. Craviso,<sup>3</sup> and Nelson G. Publicover<sup>4</sup>

<sup>1</sup>Department of Electrical Engineering, <sup>2</sup>Biomedical Engineering Graduate Program,

<sup>3</sup>Department of Pharmacology, and <sup>4</sup>Department of Physiology and Cell Biology,  
University of Nevada, Reno, Nevada

Identifying distortions produced by commonly employed microscope objectives and their components in uniform DC and 60 Hz AC magnetic fields is important in imaging studies involving exposure of cells to spatially uniform or nonuniform magnetic fields. In this study, DC and 60 Hz AC magnetic flux densities were numerically computed in the presence of finite element models of various components of commonly utilized microscope objectives, as well as a model of a complete objective. Also computed were the distortions in the current density induced by an applied time-varying magnetic field in a physiological buffer contained within a Petri dish. We show that the magnetic flux density could be increased up to 65% in the presence of the nickel–chrome plating of an objective housing and that the presence of ferromagnetic components like a screw or spring could produce peaks that are 7% higher than the undistorted value of magnetic flux density. In addition, a slight tilt of 1% in the objective with respect to the magnetic field could cause a 93% deviation in magnetic flux density from the unperturbed value. These results correlate well with previously published experimental measurements that showed the presence of significant and sometimes asymmetric distortions in both DC and 60 Hz magnetic fields. Moreover, this study further reports that induced current density changed up to 37% compared to values in the absence of the objective. The existence of distortions in applied magnetic fields and induced currents could affect the interpretation of results of cell function studies if it is assumed that the cells are exposed to uniform magnetic flux densities in the presence of a microscope objective. Such assumptions of uniform magnetic flux density could also account for the lack of reproducibility in several studies that examined changes in intracellular calcium by imaging techniques. *Bioelectromagnetics* 22:463–469, 2001. © 2001 Wiley-Liss, Inc.

**Key words:** finite element method; microscope objectives and components; magnetic flux density; DC field distortions; AC field distortions

## INTRODUCTION

The use of imaging techniques to study the effects of low frequency electromagnetic fields on cellular functions has spurred an interest in understanding the effects that microscope objectives have on magnetic field uniformity. Liburdy [1995] was the first to suggest the possibility of distortions in DC magnetic fields in the presence of commercially available microscope objectives. He was able to measure a significant perturbation in the DC magnetic field in the presence of several commercially available microscope objectives and attributed this to the presence of ferromagnetic materials in these objectives. Lindstrom et al. [1995] measured small distortions in the 50 Hz magnetic field within their exposure region in the

presence of a microscope and attributed this to metallic structures within the microscope stage.

Publicover et al. [1999] carried out a systematic and detailed experimental assessment of the distortions

---

Contract grant sponsor: NIEHS; Contract grant number: RO1 ES07563; Contract grant sponsor: NIH; Contract grant number: RO3 ES08903; Contract grant sponsor: National Science Foundation Nevada EPSCoR Cooperative Agreement; Contract grant number: OSR-9353227.

\*Correspondence to: Indira Chatterjee, Department of Electrical Engineering, University of Nevada, Reno, NV89557.  
E-mail: indira@ee.unr.edu

Received for review 8 June 2000; Final revision received 5 January 2001

in uniform AC and DC magnetic fields generated by several commonly employed microscope objectives with magnifications ranging from  $1\times$  to  $100\times$ . These measurements identified several microscope objective components made of ferromagnetic materials that contribute to magnetic field distortions. These include the nickel-chrome plating of objective housings, steel springs in objectives with compression collars and steel screws or studs used to hold together separately manufactured parts. Steel springs and screws caused asymmetric field distortions in a uniform applied magnetic field. In “simple” objectives in which no springs, steel screws, or any other ferromagnetic parts were present, distortions were produced by the nickel-chrome alloy coatings on their outer surfaces. In the case of high magnification, low working distance microscope objectives, which contain a spring mechanism, a large spatial gradient was measured in the magnetic flux density in the image plane. Another finding of this work was that in the presence of small screws that fasten together different components within the housing of more complex microscope objectives, the distortion in the magnetic field was axially asymmetric and could therefore produce a preferred direction for biological responses.

Given the importance of understanding the contribution of various microscope objective components to the distortions in the magnetic field and induced currents and the effects these may have on exposure outcomes, this numerical study was undertaken to provide a higher spatial resolution of the distortions in the magnetic flux density and induced currents than can be obtained by experimental measurements. The finite element method was used to compute the magnetic flux density in a Helmholtz coil exposure system as well as the induced current density in a Petri dish containing a physiological buffer in the presence of the various components of commonly used microscope objectives, shown by Publicover et al. [1999] to produce distortions. The numerical results not only confirmed the experimental measurements of distortions produced by microscope objectives containing ferromagnetic components, but also demonstrated that the induced current density was significantly altered.

## METHODS

Most imaging studies have used a Helmholtz coil exposure system to generate a uniform magnetic field to expose cells. Therefore, this exposure system was modeled in the computations. The objective and its components were oriented in the inverted microscope configuration, where the objectives are located beneath

a Petri dish, viewing upward. A finite element model of the Helmholtz coil magnetic field exposure system shown in Figure 1 was created. This exposure system was identical to the one being used in our laboratory for conducting fluorescence imaging experiments for the study of intracellular calcium changes in chromaffin cells [Craviso et al., 1997]. It consisted of circular coils having a radius of 5 cm with rectangular cross-sectional dimensions of  $8\times 7$  mm and separated by a distance of 5 cm as required by Helmholtz coil theory for obtaining a relatively uniform magnetic field in the central plane between the coils [Reitz and Milford, 1960]. The current (3 Ampere-turns) through the coils (same direction in both coils) in each case was that required to produce a magnetic flux density of 5.36 Gauss at the center point between the Helmholtz coils in the absence of any objective, objective components, and Petri dish.

## Numerical Simulations

The following cases were considered, based on those used by Publicover et al. [1999]:

1. A hollow nickel cylinder (shown in Fig. 1)
2. A steel spring (shown in Fig. 2)
3. A steel spring and steel screw (shown in Fig. 2)
4. A complete objective with a nickel-chrome coating on its brass housing, which was in the shape of a cylinder with a V-shaped brass cap on it, a steel screw, and steel spring (shown in Fig. 2). The objective was aligned with the vertical magnetic field.

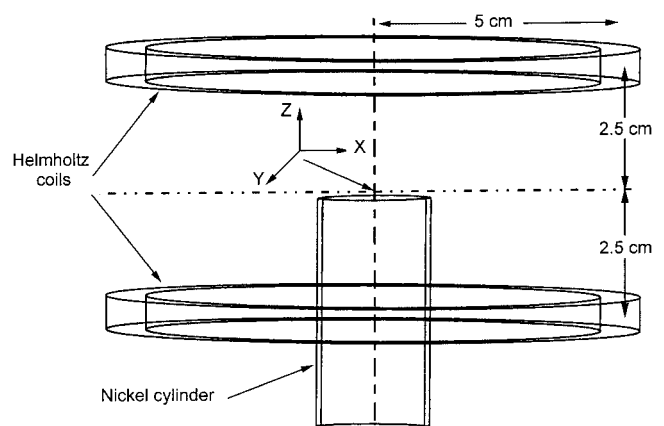


Fig. 1. Geometry of the Helmholtz coil exposure system. Cross-sectional dimensions of windings =  $8\times 7$  mm. Also shown is the geometry and position of a hollow nickel cylinder (inner radius = 7.5 mm, outer radius = 9.5 mm, length = 39 mm).

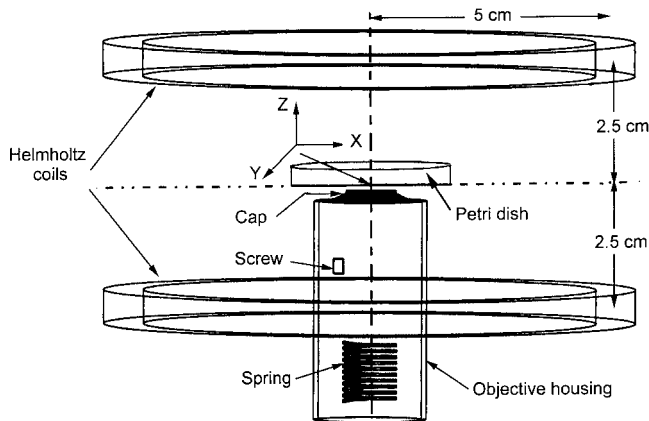


Fig. 2. Geometry of the Helmholtz coils, an objective consisting of a cylindrical brass housing (inner radius 10.5 mm, outer radius 11.5 mm) coated with a nickel-chrome layer of thickness  $4\ \mu\text{m}$ , a brass cap, compressed steel spring (length = 12 mm., number of turns = 10, inner radius = 5 mm, outer radius = 5.5 mm), steel screw (length = 2 mm, diameter = 3 mm) and a Petri dish (diameter = 34 mm).

5. Same as 4 except that the objective was tilted at an angle of  $1^\circ$  with respect to the vertical magnetic field.
6. A complete objective as described in 4, placed directly below a 34 mm Petri dish (shown in Fig. 2) containing a physiological balanced salt solution.

In all the above cases, the objective and components were placed at a location that each normally occupies in an inverted microscope viewing cells in a Petri dish. In cases 2 and 3, the spring and screw were placed 31 mm and 14 mm below the central plane respectively and the objective housing was not considered in the computations. In cases 1–5, magnetic flux density was computed whereas in case 6, the induced current density in the physiological salt solution was computed as well.

### Maxwell 3D Field Simulator

The Maxwell<sup>®</sup> 3D Field Simulator (Ansoft Corporation, Pittsburgh, PA) is an interactive software package that permits an analysis of electrostatic, magnetostatic and time-varying magnetic fields for three-dimensional structures using the finite element method to solve Maxwell's equations [Maxwell 3D, 1993]. The work presented in this paper used both the magnetostatic and time varying (eddy current) solvers. The software takes as input the geometry of the object being modeled, material properties such as magnetic permeability and electrical conductivity, sources of current or magnetic field and the appropriate electromagnetic boundary conditions describing field beha-

avior. The mesh generation capability of the software was used to create a three-dimensional finite element mesh, consisting of various sizes of tetrahedra, of the objects under consideration. Both manual and automatic or adaptive mesh refinement were utilized to obtain the best representation of the objects being modeled, especially in regions having small dimensions and/or where the geometry changed rapidly. Once a satisfactory mesh was obtained, a solution was run until the convergence criterion was met. The convergence criterion was based on the difference in the electromagnetic energy density calculated in two successive iterations being less than an operator selected preset value. Results were observed in the postprocessor. In the magnetostatic (DC) cases, the output of the software was the magnetic flux density in the region between the Helmholtz coils. In the time varying or eddy current case (60 Hz), the solution of interest was the magnetic flux density as well as induced current density in the physiological buffer placed in the Petri dish.

## RESULTS

### Computation of the Magnetic Flux Density Due to the Exposure System

In the central plane between the coils, along the y-axis shown in Figure 1, the numerically computed magnetic flux density was compared to the magnetic flux density predicted by Helmholtz coil theory (Fig. 3) [Nagaoka, 1921]. The values agreed to within 3.6% at the central point between the coils. This difference is small, considering that a comparison is being made between a numerical technique and an analytical one that involves elliptic integrals of the first and second kind that are computed via their power series representations. Including terms up to the sixth order in the series was sufficient to attain the limit of practical accuracy. For the region around the center point between the coils, where a 34 mm diameter Petri dish with cells would be placed (vertical dashed lines in Fig. 3), the magnetic flux density was uniform to within 0.2%.

### Computation of the Magnetic Flux Density in the Presence of Various Microscope Objective Components

**Hollow nickel cylinder.** As a first step in quantifying the effect of various components of commonly used microscope objectives, a finite element model of a hollow nickel cylinder (inner radius = 7.5 mm, outer radius = 9.5 mm) was created using a length (39 mm) similar to that of a microscope objective. As shown in

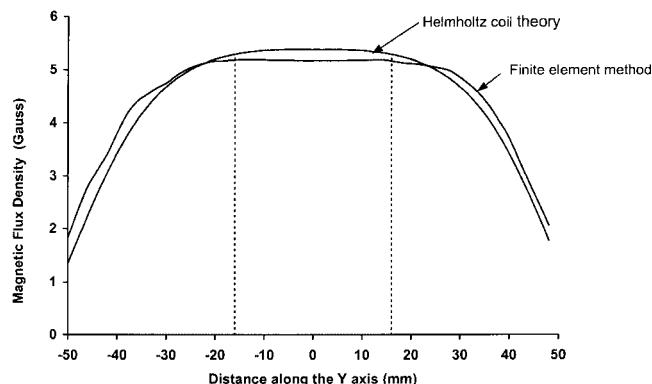


Fig. 3. Comparison of the magnetic flux density produced by a pair of Helmholtz coils in the central plane between the coils of Figure 1, obtained using Maxwell 3D and from Helmholtz coil theory. The magnetic flux density is plotted along the y-axis in the central plane between the coils. Dashed vertical lines show the region in which a Petri dish would normally be located.

Figure 1, the nickel cylinder was placed in the magnetic field created by the Helmholtz coils, 1 mm below the midplane between the coils. The thickness of the cylinder (2 mm) was large compared to the thickness ( $4 \pm 1 \mu\text{m}$ ) of the nickel-chrome coating normally found on the housing of microscope objectives like the Olympus  $10\times$  and Nikon  $40\times$ . However, it would be extremely difficult to sample over distances of the order of microns. Therefore, the computation performed with the thicker nickel cylinder allowed us to identify the distortion produced by a realistic thickness of the nickel-chrome coating in the presence of other components of an objective that also contribute to the distortions. Figure 4 shows the magnetic flux density along the y-axis (shown in Fig. 1), 1 mm above the cylinder. Results for both DC and 60 Hz are shown. In both cases there were two distinct peaks corresponding to the locations of the shell of the hollow nickel cylinder. This result is expected, since nickel has a relative permeability of 600 and tends to concentrate the magnetic flux in the shell of the hollow cylinder. In the case of DC a higher distortion was obtained (270% higher than the unperturbed value as compared to 223% in the case of 60 Hz), as would be expected from Lenz's law, which states that the induced emf (electromotive force) for time-varying fields is in such a direction as to oppose the change in the magnetic flux inducing the emf [Iskander, 1992].

**Steel spring.** In order to quantify the effect of a compressed steel spring similar to that present in high magnification, low working-distance microscope objectives for focusing (example, Edmund-Scientific  $20\times$ ), a finite-element model was created of a steel spring

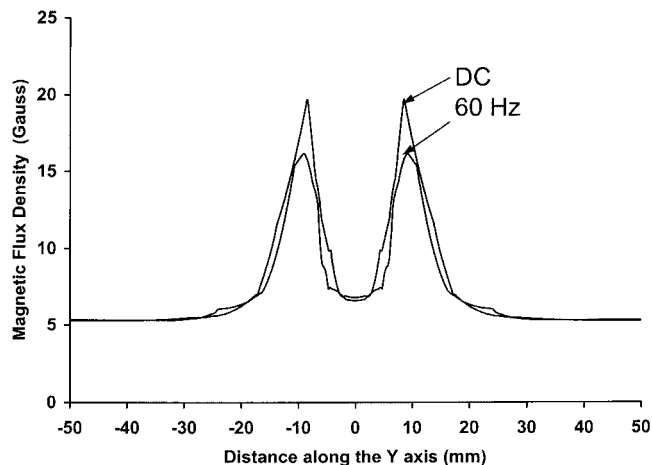


Fig. 4. Computed DC and 60 Hz magnetic flux density along the y-axis, 1 mm above the hollow nickel cylinder shown in Figure 1.

having 10 turns, inner radius = 5 mm, outer radius = 5.5 mm, length 12 mm and relative magnetic permeability of 2000. The dimensions of the spring corresponded to those in a compressed state inside an objective. The geometry and location of the spring is shown in Figure 2, and a plot of the magnetic flux density along the y-axis in the central plane is shown in Figure 5 for both DC and 60 Hz. Two peaks higher than the unperturbed value were observed corresponding to the locations of the steel in the spring. The maximum deviation of the magnetic flux density from the unperturbed value of 5.36 G was 3.3% at the peak for DC and 2% at 60 Hz. The magnetic flux density at the peaks for 60 Hz was lower than that at DC due to the opposing magnetic field set up by the induced eddy currents in the steel.

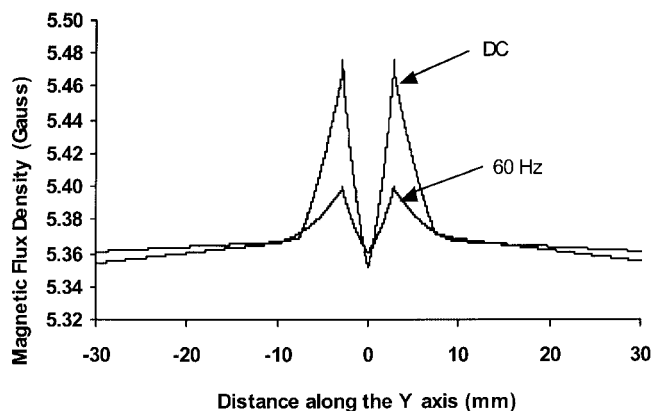


Fig. 5. Computed DC and 60 Hz magnetic flux density along the y-axis, 31 mm above the compressed steel spring shown in Figure 2.

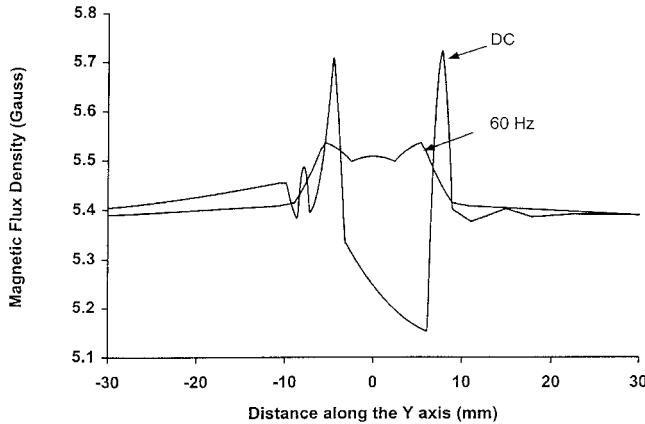


Fig. 6. Computed DC and 60 Hz magnetic flux density along the y-axis above the compressed spring and screw shown in Figure 2 (the spring and screw are 31 mm and 14 mm below the y-axis respectively).

**Steel spring and screw.** Figure 2 also shows the geometry and location of a steel screw that would normally occur in an actual microscope objective in which small screws or slugs are used to fasten together different components within the housing. The screw was 2 mm in length and 3 mm in diameter. The results of the magnetic flux distortion at DC and 60 Hz produced in the presence of the compressed spring and screw are shown in Figure 6. Three DC peaks were present, the smaller one on the left corresponding to the screw and the two larger ones corresponding to the spring. The asymmetric dip in the magnetic flux density is attributed to the presence of the screw. The deviation of the highest peak from the unperturbed value of magnetic flux density was 7% at DC. The peaks due to the spring at 60 Hz showed a deviation of 2.7% from the unperturbed value and the peak due to the presence of the screw was not noticeable.

**Complete objective.** A complete objective, as depicted in Figure 2, was modeled using the aforementioned ferromagnetic components (steel screw and compressed spring) at their appropriate locations inside a brass housing (hollow cylinder of inner radius 10.5 mm and outer radius 11.5 mm). A thin coating of nickel-chrome of thickness 4  $\mu\text{m}$  covered the housing. In addition, a cap made of brass was placed on the brass cylinder. No glass components of the objective were included since glass, being a non-magnetic material, is not expected to perturb the magnetic field. The DC and 60 Hz magnetic flux density along the y-axis, 2 mm above the microscope objective are shown in Figure 7. The two higher peaks were due to the thin nickel-chrome coating, whereas the smaller perturbations were due to a combination of the effects of the steel

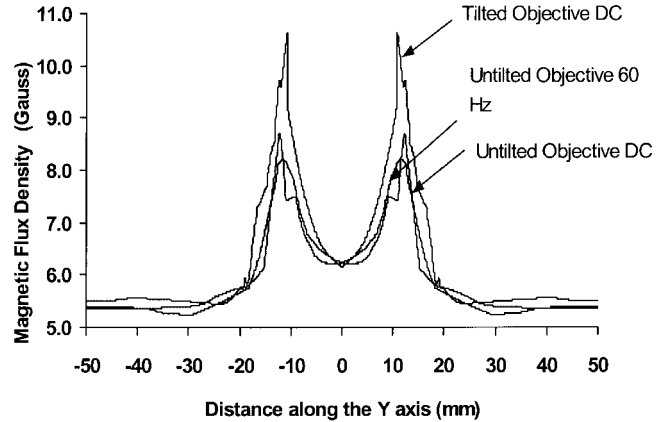


Fig. 7. Computed DC and 60 Hz magnetic flux density along the y-axis, 2 mm above the objective shown in Figure 2, for the case of no tilt and DC magnetic flux density for the case of a 1° tilt of the objective (with respect to the vertical magnetic field).

screw and spring. The maximum deviation of the magnetic flux density from the undistorted value of 5.36 G was 65% at the higher peaks. This was much less than that obtained with the nickel cylinder which had a much larger thickness of nickel than the nickel-chrome coating and hence created a larger concentration of magnetic flux right above the cylinder shell.

To evaluate the effect on magnetic field distortion due to a slight tilt in the objective such as might occur during the process of mounting the microscope system, the complete objective was also modeled giving it a 1° tilt with respect to the direction of the vertical magnetic field. As shown in Figure 7, the maximum deviation of the magnetic flux density from the unperturbed value of 5.4 G was 93%, which is a 1.4 fold increase over that obtained when the objective was not tilted. A worst-case tilt of 10° was found to produce an asymmetry in the peaks with the higher peak on the side of the tilt (data not shown).

### Computation of the Induced Current Density in a Petri Dish Containing a Physiological Buffer

The time-varying magnetic field or eddy current solver of Maxwell 3D was used to create a finite-element model of a 34 mm diameter Petri dish placed in the central plane between the Helmholtz coils as shown in Figure 3. The dish contained a 4 mm height of a physiological buffer whose electrical conductivity was assumed to be 1.5 S/m [Bassen et al., 1992]. The objective was placed 2 mm below the Petri dish in the “inverted microscope” position. Figure 8 shows the induced current density along a radial line (y-axis) from the center to the edge of the Petri dish. Also shown in Figure 8 is the theoretically calculated

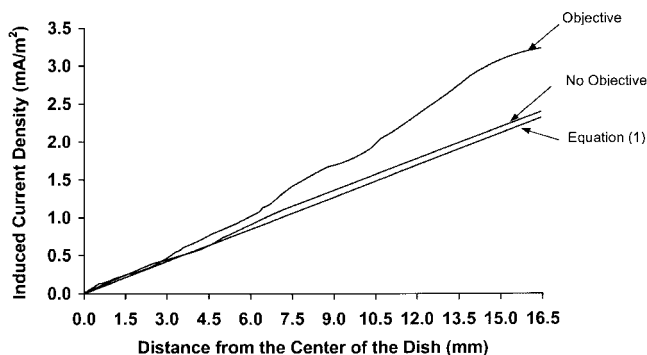


Fig. 8. Comparison of the computed induced current density in the Petri dish in the presence and absence of the objective. Values were obtained along a radial line from the center to the edge of the Petri dish. Also shown is the theoretically predicted current density using equation (1).

induced current in the Petri dish obtained from the equation [Bassen et al., 1992]:

$$J = \pi \sigma, f B r \quad (1)$$

where

$\sigma$  = electrical conductivity of the physiological buffer

$f$  = frequency of the magnetic field

$B$  = magnetic flux density

$r$  = radial distance from the center of the Petri dish

The agreement in Figure 8 between the numerically and theoretically calculated current density was very good (to within 1.6%).

In the presence of the objective, the current density in the Petri dish was higher than in the absence of the objective. Moreover, as the radial distance from the center of the dish increased, the difference  $\Delta J$  in current density with and without the objective increased to a maximum value of 1 mA/m<sup>2</sup>. This value represented a 37% change in the current density attributed to the presence of the objective. A three-dimensional plot of the difference  $\Delta J$  in induced current density in the presence of the objective and in the absence of the objective, due to the 60 Hz applied magnetic field, is shown in Figure 9. This figure shows the larger current density present in the presence of the objective in the region that would normally be occupied by a Petri dish.

## DISCUSSION AND CONCLUSIONS

The numerical computations presented in this paper have quantified the distortions produced in a DC and 60 Hz uniform magnetic field by (1) various ferromagnetic and metallic components typically found

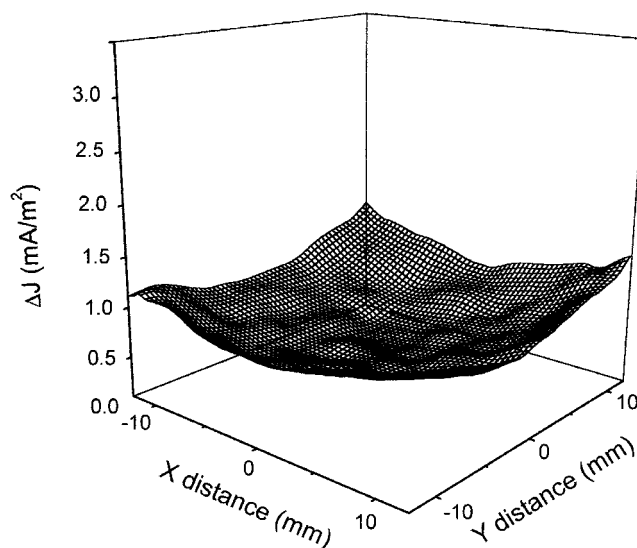


Fig. 9. Three-dimensional plot of the difference  $\Delta J$  between the induced current density in the presence of the objective and in the absence of the objective in the region normally occupied by a Petri dish.

in microscope objectives and (2) a complete objective containing a steel spring, steel screw, and nickel-chrome coating on a brass housing. In all cases, the distortions are lower at 60 Hz as compared to DC, consistent with Lenz's law [Iskander, 1992]. The effect of a slight tilt of the objective with respect to the magnetic field was also computed. We have also quantified the distortion in the current density induced at 60 Hz in a physiological buffered salt solution contained in a circular Petri dish, produced by the presence of the complete objective. The results have not only confirmed that the specific cases mentioned above produce significant distortions in the magnetic flux density both at DC and 60 Hz, but also more importantly demonstrate the effect that they have on the current induced in Petri dishes containing physiological buffer medium. In addition, we have demonstrated that it is possible to obtain a degree of spatial resolution in the numerical computations that would be difficult with measurements that are limited by probe size. This would be very important particularly when assessing the distortions produced in magnetic flux density and/or induced current density in small regions where cells may be located in a Petri dish.

In the case of the nickel cylinder placed in the uniform magnetic field, the magnetic flux density above the cylinder is no longer uniform and the field can be increased by up to 270% of the unperturbed uniform value in the case of DC fields and up to 223% in the case of 60 Hz fields in the region normally occupied by the bottom of a Petri dish containing a cell

preparation. Publicover et al. [1999] found a similar peak and valley behavior of the magnetic flux density for measurements on an actual Olympus 10 × objective which had a nickel–chrome coating on its housing.

A comparison of our results in the case of the compressed steel spring in a uniform magnetic field with those of Publicover et al.[1999] using an uncompressed spring pointed out that the asymmetric peak observed by them disappeared when a compressed spring was present. This was because the compressed spring more closely resembled a hollow steel cylinder. Thus, the degree of asymmetry depends on the focusing characteristics of the objective, which relates in turn to different degrees of compression.

When both a steel spring and screw were present, the magnetic flux density was radially asymmetric due to the presence of the embedded steel components. This result agreed with those measured by Publicover et al.[1999]. The maximum deviation of the DC magnetic flux density from the undistorted value of 5.4 G was 7% at the higher peaks corresponding to the spring.

In the case of the complete objective, higher peaks were observed when the objective was tilted with respect to the vertical magnetic field. This was because the tilt caused a larger area of the objective nickel–chrome coating to intercept the magnetic flux lines and hence a greater concentration of magnetic flux in the region above the objective. Publicover et al. [1999] reported a similar observation. Thus, precise alignment of an objective containing ferromagnetic components is important in imaging studies.

Finally, the larger induced current density obtained in the presence of the objective is expected, based on the large distortion present in the magnetic flux density due to the nickel–chrome coating. This resulted in the physiological buffer in the dish being exposed to a larger magnetic flux density further away from the center of the dish. Thus, cells would be exposed to different magnetic flux densities and induced current densities depending on their location in the Petri dish. This would in turn distort the induced current density from its value in the presence of a uniform magnetic flux density. This distortion effect would be significant in interpreting results of cell functions using an inverted microscope system where

researchers usually assume that the cells are exposed to a uniform magnetic flux density. It may also affect the reproducibility of results obtained by different researchers. Finally, even if externally applied magnetic fields are not present, numerous studies are performed in the presence of the earth's DC magnetic field. The distortions demonstrated might affect the outcome of such studies.

## ACKNOWLEDGMENTS

Part of this research was supported by grants from the NIEHS/DOE RAPID program through NIH (RO3 ES08903) and NIEHS (RO1 ES07563). Noha Hassan was supported through funds from the National Science Foundation Nevada EPSCoR Cooperative Agreement OSR-9353227.

## REFERENCES

- Bassen H, Litovitz T, Penafiel M, Meister R. 1992. ELF in vitro exposure systems for inducing uniform electric and magnetic fields in cell culture media. *Bioelectromagnetics* 13:183–198.
- Craviso GL, Lundback SS, Chatterjee I, Publicover NG. 1997. Fluorescence imaging of intracellular calcium levels in primary cultures of adrenal chromaffin cells during exposure to 60 Hz EMFs. Twentieth Annual Meeting of the Bioelectromagnetics Society. St. Pete Beach, FL, June 7–11, 196 p.
- Iskander, MF. 1992. *Electromagnetic Fields and Waves*. Prospect heights, IL: Waveland Press, Inc.
- Liburdy RP. 1995. Microscope objectives perturb local dc magnetic fields; a factor in EMF microscopy studies. Seventeenth Annual Meeting of the Bioelectromagnetics Society. Boston, MA, June 18–22. 42 p.
- Lindstrom E, Lindstrom P, Berglund A, Lundgren E, Mild KH. 1995. Intracellular calcium oscillations in a T-cell line after exposure to extremely low-frequency magnetic fields with variable frequencies and flux densities. *Bioelectromagnetics* 16:41–47.
- Maxwell 3D field simulator user's reference. 1993. Pittsburgh, PA: Ansoft Corporation.
- Nagaoka H. 1921. Magnetic field of circular currents. *The Philosophical Magazine* 41:377–388.
- Publicover NG, Marsh CG, Vincze CA, Craviso GL, Chatterjee I. 1999. Effects of microscope objectives on magnetic field exposures. *Bioelectromagnetics* 20:387–395.
- Reitz JR, Milford FJ. 1960. *Foundations of electromagnetic theory*. Reading, AM: Addison-Wesley Publishing Co., Inc.